Journal of Engineering and Applied Science

RESEARCH Open Access

An impact echo method to detect cavities between railway track slabs and soil foundation

Pierre Anthyme Bahati*, Viet Dinh Le and Yujin Lim

* Correspondence: bahatipierreanthyme@gmail.com
Department of Civil and Railroad Engineering, PaiChai University, Daejeon, South Korea

Abstract

The impact echo technique is one of the most useful non-destructive test methods for determining the thickness of concrete or detecting possible cracks or cavities in the internal parts of a concrete structure without damaging the surface. Many types of unstable conditions in railway tracks, including various modes of irregularities, may occur when cavities are generated directly under a concrete slab track or when a slight open space is made under a loose sleeper. In this study, we developed a nondestructive testing (NDT) system for detecting abnormalities in concrete tracks and performed 3D numerical simulations using the ABAQUS finite element analysis (FEA) program to investigate the impact echo response from a concrete track slab with different sizes of cavities. Sections of concrete slab were simulated as solid body masses under the railway tracks with gaps in the bodies themselves or with cavities existing between the track concrete layer (TCL) and the hydraulically stabilized base (HSB). We investigated the locations and depths of the cavities and gaps in the model concrete slab using the acoustic impact echo response based on the frequency response of the elastic waves generated in the slab. In addition, a Short-time Fourier Transform (STFT) and a wavelet technique were adopted for a time frequency analysis. Our study demonstrated that the impact echo technique developed in this study by FEA and NDT can measure and confirm the location and depth of cavities in concrete slabs.

Keywords: Concrete slab track, Impact echo, Finite element analysis, STFT, Wavelet

Introduction

Research background and purpose

A slab track is a concrete or asphalt reinforced layer that replaces the crushed stone layer of the standard ballasted track. The first slab track systems appeared long ago, approximately at the beginning of the twentieth century, but their extensive development and use started in the 1970s [1, 2]. The increased railway speeds nowadays are making the slab track concept more attractive than ever before. Most developed and many developing countries in the world have high speed lines running at speeds of

over 300km/h, and they are planning to upgrade their existing lines or to create new high speed railway routes [3].

Many types of unstable conditions in railway slab tracks, including various modes of irregularities, can be produced when cavities are generated exactly underneath a concrete slab track or a slight open space is made under a loose sleeper [4]. Cavities may be generated from several causes, for example settlement of badly compacted soil or soft original ground soil or a drastic change in track stiffness in transition zones near a bridge abutment. Nonetheless, there are currently no useful and effective detection methods for investigating the presence of cavities under the railway concrete slab track and the loose sleeper embedded in the slab.

Impact-echo (IE) is a non-destructive test method for evaluation of concrete structures based on the propagation and interaction of mechanically induced stress waves in the concrete medium. It has a wide range of applications from quality control (thickness measurement, grouting in tendon ducts, epoxy injected in surface opening cracks, etc.) to defect characterization (location, shape and size of voids, surface opening cracks, delamination, etc.) [5].

New technologies such as stack imaging of spectral amplitude based on impact echo (SIBIE) [6] and rapid data acquisition through multisensory [7] and contactless sensing [8, 9] have been used to improve the process and quality of defect characterization using the IE method. Various numerical techniques like the finite difference time domain (FDTD) and finite element method (FEM) have been employed to simulate the impact echo response of various concrete, reinforced, and composite structural components. These techniques are based on the fundamental theory of elastic stress-wave propagation in an infinite elastic solid and have been successfully applied over a wide range of sections with complex geometric and boundary constraints [1, 6–9].

In this study which is based on Master's thesis [1] has been upgraded and improved dramatically, we were the first to design a new impact echo testing system for detection of cavities under concrete track slabs with a new automatic impacting and measurement system configured for detecting the position of irregularities and abnormalities under or in the concrete track slab.

Furthermore, we also analyzed the response of the impact echo test using wavelets and the short-time Fourier transform (STFT) of the obtained data from 3D FE analysis of ABAQUS, the general purpose FE program which we adopted to analyze many effects and aspects of cavity existence problems under the railway slab track which is loaded dynamically. A similar analyzing approach was also used by Melhem and Kim [8] and by Song and Cho [9] both for damage detection in concrete. In fact, the IE technique was deeply studied in the NDT for concrete plate and tunnel lining. The time-frequency analysis was also introduced in this area, including STFT, WT, and HHT. The detailed procedures for performing STFT to get wavelet forms and auto spectrum density were explained by [10].

Results and discussion

Methodology

In this study, we developed a system to measure the vibration generated by an impact load applied mechanically on the surface of a layered concrete bed using an

accelerometer. The developed defect measurement system is based on impact echo and consists of an impact loading transmitter composed of a solenoid and a receiver equipped with an NI DAQ board and an accelerometer. All important working parts were installed together in a trigger kit box as shown Fig. 1a. The loading transmitter is activated by a control switch that triggers the solenoid rod to generate an impact force.

A touch screen panel (Fig. 1b) was added to a separate control box for data processing and data analyzing and to obtain wavelets and the STFT. A small computer board was installed in a separate main box for this purpose. The trigger box was connected to the main box via electric wires.

Stress wave

As generally known, if a shock is applied to a hard surface of solid material such as concrete, a compressive wave (P), a shear wave (S), and a surface wave (R) are emitted from the impact source as shown below (Fig. 2). The impact echo technique uses the P wave with a constant propagation velocity at all frequency components among the three stress waves. The velocity (v) is determined by the stiffness (E or G) and mass density (ρ) of the material. The propagation velocity (Vp) of the P wave can be expressed as the product of the frequency (f) and the wavelength (λ).

When wave propagation comes into contact with a surface with different properties, a reflection occurs due to the difference in impedance at the interface. In particular, the difference in acoustic impedance value between the concrete slab and the cavity increases considerably when a cavity and lifting occurs on the bottom surface of the concrete slab, so that the surface of adhesive bonds with the concrete becomes a single reflection surface.

In this case, the upper space of the concrete slab is an air layer, and the lower surface is also a free-free boundary system because the air layer is formed by the cavity. The resonance of the primary mode at the free ends in both end surfaces occurs when the wavelength λ becomes twice the depth or thickness d.

$$\lambda = 2d \tag{1}$$

Thus, if the P wave velocity (Vp) of the concrete slab in the measurement section is known, the measured resonance frequency (f) can be used to determine the depth (d) of the cavity, which is shown in Eq. (2).

(a) (b)

Fig. 1 The main body of the impact echo device and touch screen panel

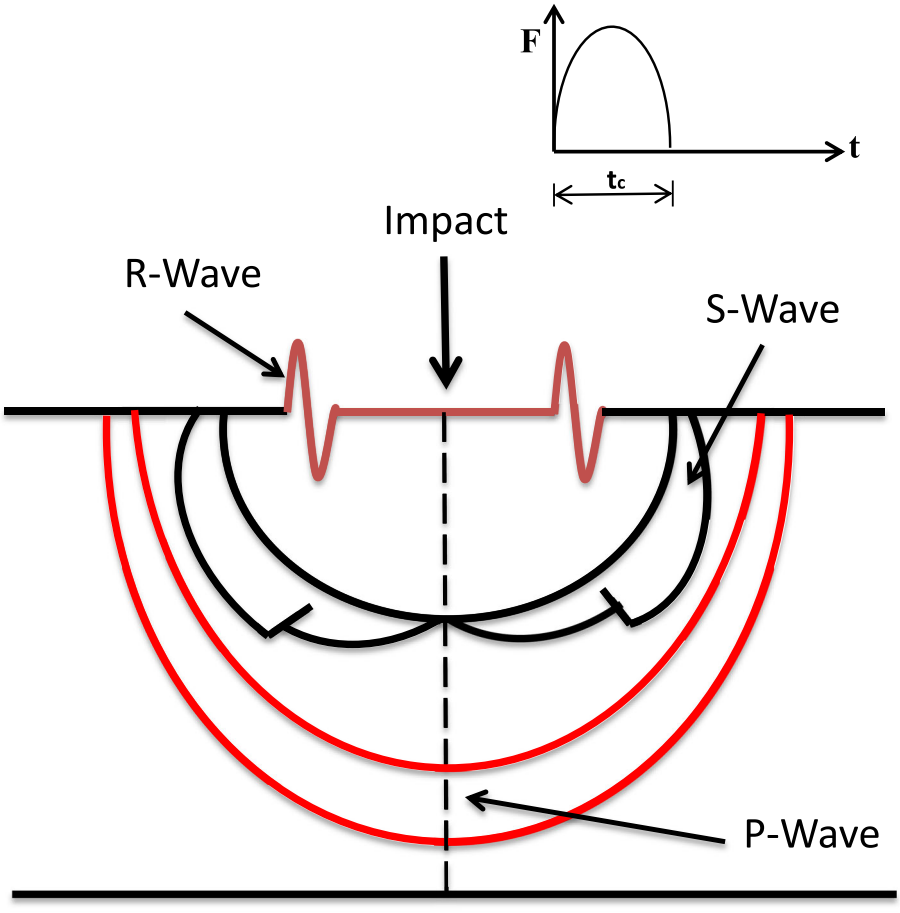

Fig. 2 Wave generation and propagation by impact load

$$d = \frac{V_{p\,\max}}{2f} \tag{2}$$

Sansalone [4] concluded that the concrete slab thickness calculated by Eq. (2) differed by about 5%. In case of multiple reflections of P waves, the so-called thickness mode is generated so that Eq. (2) is expressed as (3) using the shape coefficient (β). In this study, the shape factor of the concrete slab was selected as 0.96 as proposed by Sansalone [5].

$$d = \frac{\beta v_{p\,\max}}{2f} \tag{3}$$

Time-frequency analysis using wavelet technique

Fourier transform is one of the most widely used techniques in signal processing. It divides the measured signal into several sine waves with different frequency components. Since this technical process evaluates the average frequency characteristic within the total period of the measured signal, time information is lost for a signal whose frequency characteristic changes with time [9] (Fig. 3).

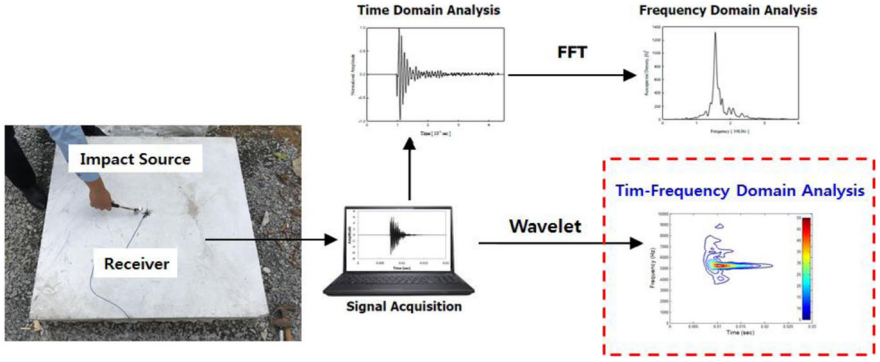

Fig. 3 Time-frequency analysis process

In other words, it is not suitable as a method for identifying the change of characteristics in the frequency spectrum with time. In order to overcome these limitations, a time-frequency analysis technique has been introduced [6, 8, 11, 12] that can simultaneously analyze time information and frequency information of signals.

The time-frequency analysis technique applied in this study is the short-time Fourier transform (STFT) of wavelet method. STFT is a technique for obtaining the segmented and filtered functions by applying the window function to each time band in order to obtain frequency characteristics over time and to perform the Fourier transform. The STFT signal of the stress wave obtained by the impact echo test was processed according to the following procedure [8, 9, 13, 14].

The STFT obtains only the signal of frequency component in the area where the window function is applied. It evaluates the change of the frequency component with time by shifting the window function in the time band. Therefore, the determination of the window width is an important factor in time-frequency analysis. If a narrower window width can be obtained, it is easier to evaluate the local frequency characteristics of the signal only. However, in this case, the frequency resolution decreases as the amount and cycle of time signal information contained in the window decreases. On the other hand, as the window width increases, the bandwidth of the evaluation time increases, so that it is difficult to evaluate time as the frequency resolution tends to increase [9].

In this study, the time domain analysis and the frequency domain analysis were performed independently using 1024 discrete items of signal data obtained from the test [15, 16]. The total period of the measured signal was divided into 16 intervals and 128 window data points. Time-frequency analysis was also performed.

Auto spectrum density obtained by the time-frequency analysis showed the rate of change of the spectrum with respect to the frequency. In Eq. 4, the spectral density function is the integral of the mean square value of the time domain signal across the entire frequency band. The unit is the power per unit frequency.

$$s(f) = \lim_{T\to\infty} \frac{E|X_T(f)|^2}{T} \tag{4}$$

where S (f) is the auto spectrum density, E is the expected energy, T is the time, and XT (f) is the Fourier transform value.

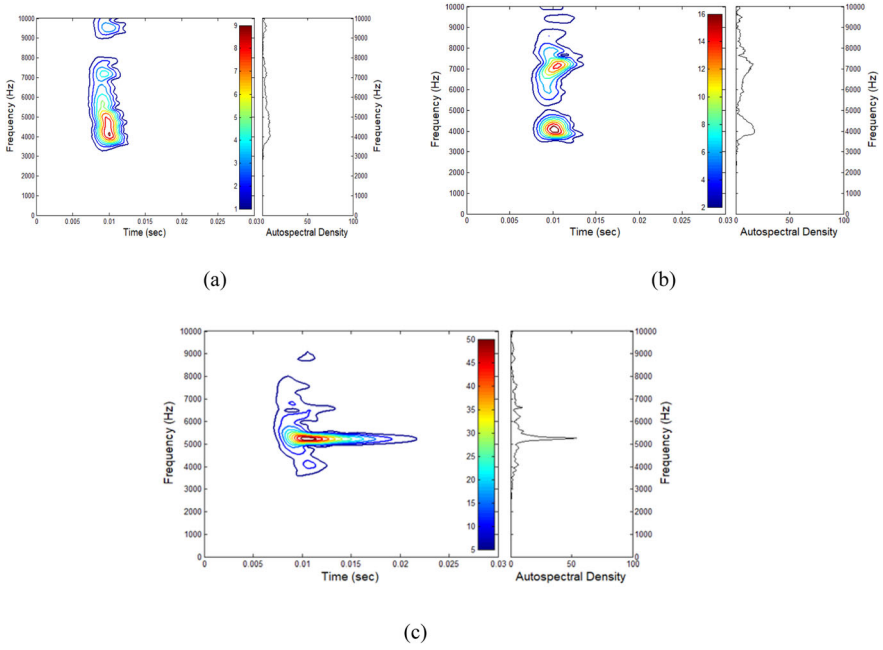

Fig. 4 Test result graph according to adhesion condition: **a** Fully bonded state. **b** Debonded state. **c** Cavity existence and abnormal state

Evaluation method of concrete track fault by signal analysis

Based on typical test results such as in Fig. 4 obtained from a small concrete slab simulated as ballast of a railway track, a plausible test procedure using the new impact echo device was designed to investigate and detect a cavity in the concrete slab track. In general, the test results from concrete slab track were evaluated in the following order: First, we checked the response spectrum in the frequency domain to determine the resonance at a specific frequency. If resonance does not occur, we moved to another position and continue the test. Second, when resonance occurs, we check the maximum value of the spectral density. If the maximum value of the spectral density is smaller than 40, we concluded that it is in a strong bonding state in the concrete slab track. However, if the maximum value of the spectral density is amplified to more than 40, we conclude that it is an abnormal section. An additional test should be done at the same position to check whether the resonance occurs and that the maximum value of the spectral density is definitively greater than 40. Third, if resonance occurs and the maximum spectral density is large enough, we check the shape of the time-frequency contours. If the shape of the time-frequency contours is long enough in the time axis direction, it is confirmed that there is a cavity or an abnormal section. In this case, the maximum spectral density is high enough and has a wider distribution.

However, if the frequency axis and the contour parallel to the time axis appear simultaneously and if the shape of the contours is independently circular or square and/or rectangular, it is mostly generated in the direction of the frequency axis, and additional testing may be needed to check the shape of contours again. This phenomenon was also observed by Song and Cho [8] and also in [17]. If the shape of the contours is circular or square/rectangular again, it is confirmed that a debonded state was generated. Fourth, even though the shape of contours in the time-frequency domain is formed

longitudinally long enough in the direction of the time axis with a flatter distribution of the spectral density, it is sure that there is no significant cavity and there is a slight possibility of cracks or similar abnormalities. Thus, in this case, resonance did not occur.

In all frequency bands in Fig. 4a, the spectral density is generally low and there is not enough maximum value to indicate a cavity, so that no reflected wave due to cavity is considered to be there. The shape of the time-frequency contour is long in the frequency axis direction only, which indicates good bonding and no cavity.

The view of Fig. 4b reveals that there is a small amount of reflected waves due to a small size cavity or excitation due to the existence of a small peak value in several frequency bands. The shape of the time-frequency graph is close to the circle, indicating that the adhesion state is poor.

In Fig. 4c, there are condensed contours generated with very high peak values in a specific frequency range. This indicates that there is a cavity at the interface between the railway concrete slab and the ground soil. The shape of the time-frequency contours is sufficiently long enough in the direction of the time axis, indicating that a cavity exists in the concrete structure.

Field test of an impact echo testing system

Bonding between concrete slab layers

Figure 5 shows the embankment section and the completed track view for the field test of the concrete defect measurement system. A TCL layer and an HSB layer were laid on the top surface of the upper part; this system used the Rheda 2000 (Vossloh System 300-1) [10, 18–22]. The TCL layer and the HSB layer were installed at the location shown in Figs. 5 and 6 by making a woodblock panel 400 mm in length and 5, 10, and 15 mm in thickness. The thickness of No. 1 woodblock was 5 mm, of No. 2 wood block 10 mm, of No. 3 wood block 15 mm, and of No. 4 wood block 5 mm.

Site impact echo system test results analysis and discussion

Figure 7 shows the impact echo test results at the upper part of the concrete after simulating the pattern between the TCL-HSB layers of the concrete track. With the

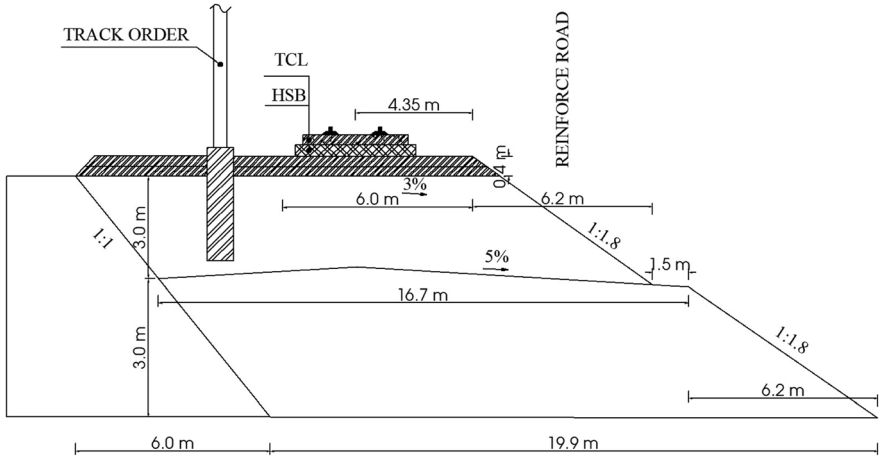

Fig. 5 Test section track view

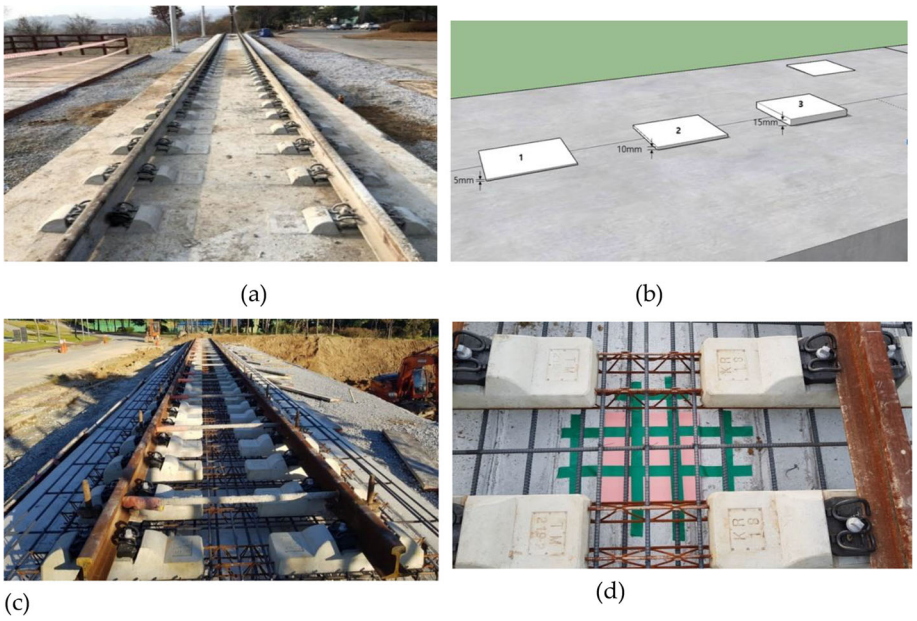

Fig. 6 Track foreground section: **a** Test section track foreground. **b** Location of wood blocks. **c** Foreground before the TCL layer was laid. **d** Wood block in the foreground

assumption that the P wave velocity (vp) of the concrete is about 1100 m/s, the shape factor (β) is 0.96 in Eq. (3), as the thickness of the woodblock becomes thicker and the resonant frequency increases slightly and the thickness of the TCL layer becomes thinner. The depth of each layer is 259 mm, 253 mm, 246 mm, and 199 mm, respectively.

The thickness measured at the center of the track was relatively more accurate than the thickness of the TCL layer, and the 4th test result was thinner than the actual thickness at the TCL side. This side test actually needs to verify the TCL layer thickness of the test location. Moreover, since the TCL is close to the outer side, it is necessary to investigate the effect of this test through further study. In this way, if there is an irregularity between the TCL layer and the HSB layer, the impact echo technique developed in this study can measure and determine the obstacle and estimate its depth.

Figure 8 shows the results of time-frequency analysis using the wavelet method. In all the test results, a relatively longer shape is seen on the time axis than on the frequency axis. In addition, the resonance frequency of the resonator is relatively long (about 8 to 10 ms), and the resonance frequency is larger in Fig. 8c and also lower in Fig. 8d which is the result of the outside of the TCL.

The spectral density value was higher than the 1600 measured at the center of the track and was the largest in Fig. 6b, in which the thickness of the wood rock was 15 mm. Table 1 compares the measured depth with the actual depth using the resonance frequency of the test result.

Finite element analysis for impact echo testing system

In this study a 3-D model of a slab track was developed using ABAQUS FEA software in order to perform an impact load analysis under dynamic loading to detect cavities under a concrete track slab.The effect of the impact load has been analyzed in different

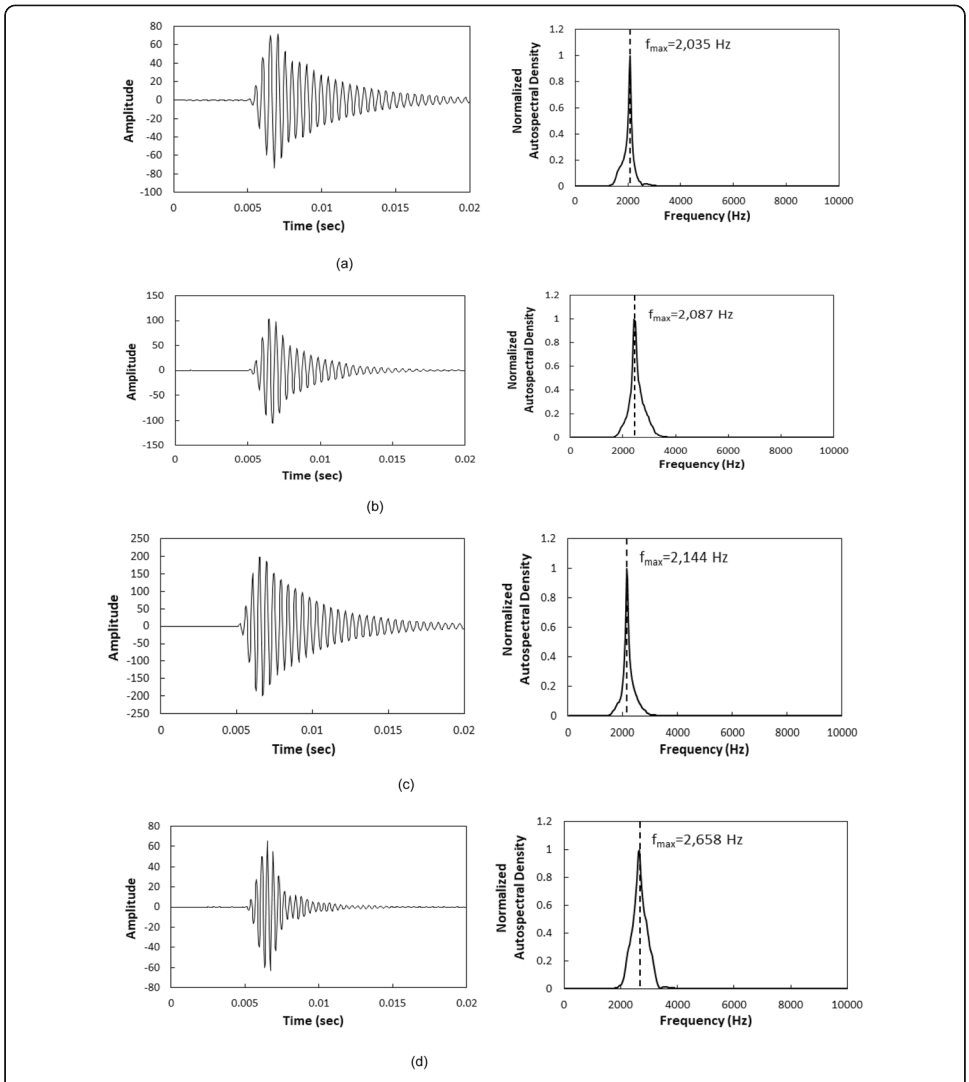

Fig. 7 Impact echo test results: **a** Station 1 woodblock thickness 5 mm. **b** Station 2 woodblock thickness 10 mm. **c** Station 3 woodblock thickness 15 mm. **d** Section 4 TCL side woodblock thickness 5 mm

positions and directions on the top of concrete slab; that is why the railway track 3-D model has been used over 2-D model.

The acceleration results were used to obtain STFT and wavelet results to detect and evaluate the effect of cavities under concrete track slabs. Three layers (TCL, HSB, Soil) were used to build a model in ABAQUS 3D.

Model's geometry

The geometry of the model is clearly illustrated in the following figures. The detailed cross section dimensions are shown in Figs. 9 and 10 and are identical to a typical [1, 10] model. Figure 9 depicts the actual model together with the basic dimensions for each layer of the track. Figure 10 shows the whole 11m long, 10m width and 5 height of 3D slab track model designed in ABAQUS. Table 2 shows the material properties used for simulating the slab track model components.

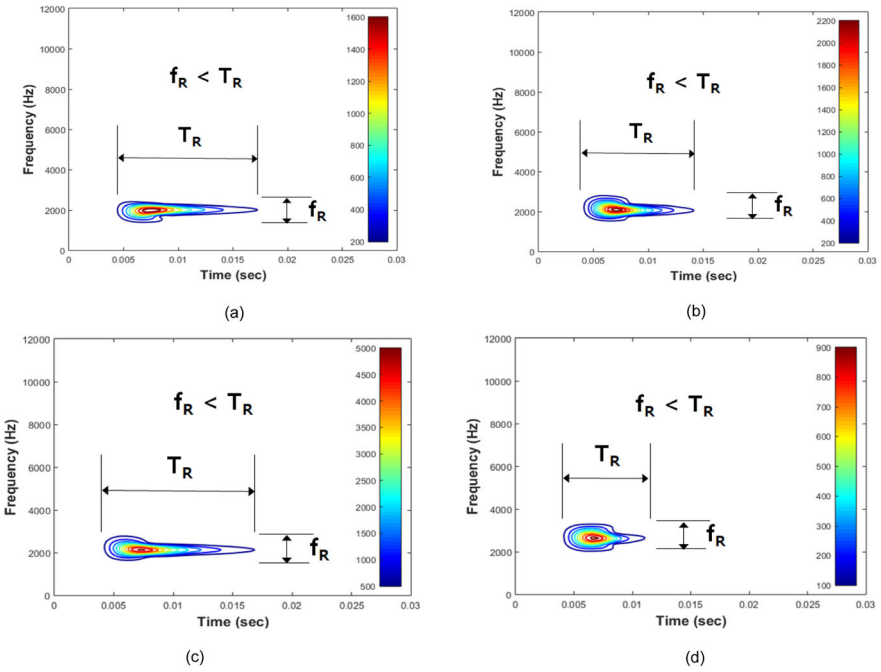

Fig. 8 Wavelet analysis result: **a** Station 1 woodblock thickness 5 mm. **b** Station 2 woodblock thickness 10mm. **c** Station 3 woodblock thickness 15 mm. **d** Station 4 TCL side woodblock thickness 5mm

Track model simulation

The three railway track layers, the TCL, the HSB, and soil, were simulated as homogeneous material and divided into two zones as shown in Fig. 10: the peripheral zone and the inside zone. The elements in the peripheral zone were expressed and set as infinite elements. The elements of the inside zone were set as 3D Plain Strain (Finite element).In addition , the infinite element has been performed here instead of using mesh or boundary conditions. This is because of Rayleigh wave which are the type of surface acoustic wave that travel along the surface of railway track when applying the impact load on it (see Fig. 2), [19, 23].

Furthermore, all the elements in the inside zone were set as square elements with a size of 5cm by 5cm (Fig. 11). The size of the elements in the peripheral zone was set to be 5cm thick and 100cm long.

The models with cavities and the models without cavities had the same input parameters. There were six different sizes of cavities (Table 3). They were modeled as 5cm × 5cm × 5cm, 5cm × 5cm × 1.25cm, 5cm × 5cm × 0.75cm, 5cm × 5cm × 0.3cm, and also cavity sizes of 40cm × 40cm × 1.5cm and 40cm × 40cm × 1cm, which were similar to

Table 1 Comparison of the measured depth and the calculated gap depth

No	Cavity Size (mm)	TCL Thickness (mm)	Calculation Gap depth (mm)	Frequency (Hz)
1	400 × 400	250	259	2035
2			252	2087
3			246	2144
4			199	2658

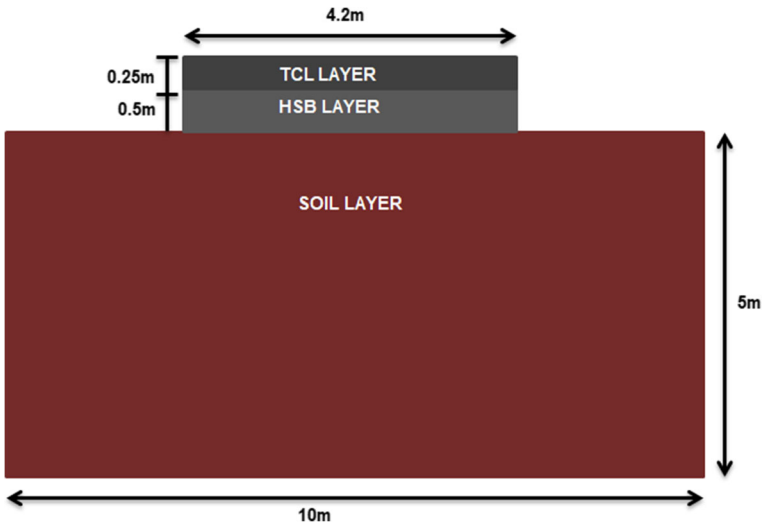

Fig. 9 Cross-section dimensions of the slab track model

the cavity size installed on field site at DongYang University, for comparing and checking the similarity between the results from FEM and the field site (Fig. 26).

Modeling for impact loading

To study the effect of cavities under concrete slabs, an impact load of 250N was applied to a 10-m long concrete slab (TCL) (Fig. 12). The impact load was applied in the center position as shown in Fig. 13, and the cavity size was localized in the middle between the TCL and HSB.

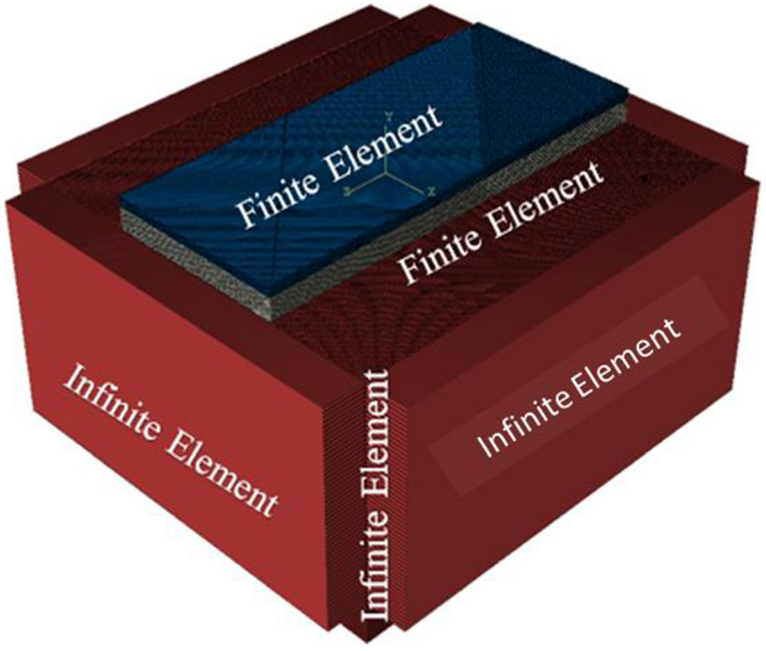

Fig. 10 Slab track model in ABAQUS

Table 2 Material properties of the railway track model components used for FEA using ABAQUS

Track Components	Unit weight, γ (kg/m^3)	Modulus of elasticity, E (Kpa)	Poisson's ratio, v	Wave velocity (m/s)
Concrete slab (TCL)	2450	3.19e+07	0.15	
Concrete box (HSB)	2445	2.58e+07	0.15	1100
Soil	2000	80000	0.3	

The impact load used in this FEA simulation of the impact on a railway concrete slab track was a half-sine curve function force as shown in Fig. 12. The loading duration is assumed to be 0.004 s. The maximum applied impact load was 250N.

Abaqus 3D simulated results analysis

Comparison of impact load for different cases of cavity size For Abaqus 3D simulated results from the impact load on a concrete slab track with and without cavities, we obtained acceleration signals with time for different sensing points as shown in Table 3 and Fig. 14. Using those acceleration signals with time, the magnitudes of the acceleration curves from the impact load were obtained in the frequency domain. First, all signal data with time were converted to the frequency domain using the FFT.

For the case where there was no cavity in the concrete slab track, the magnitude curves were obtained for different sensing points (see Table 3) and presented in case 1. It can be clearly seen for all sensing points that the first mode resonance frequency (fr) or return frequency peaks were much higher than the frequency (fd) that corresponds to the frequency of reflections from the cavity depth. Furthermore, it could be logically

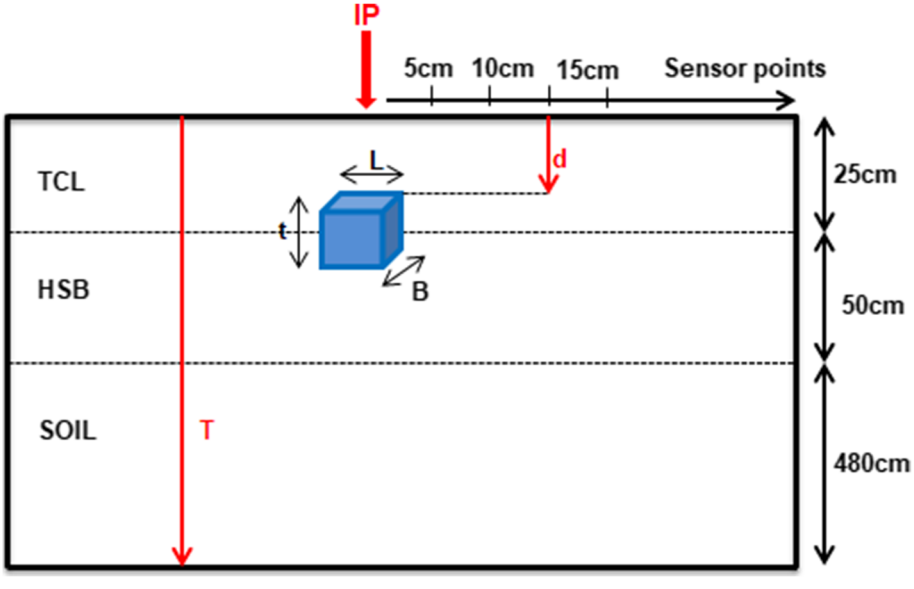

Fig. 11 Schematic for cavity location with the sensing distance

Table 3 Cavity size and sensing distance

Cavity size (cm)			Y (cm)	X (cm) Sensing distance			
t	B	L		cm	cm	cm	cm
5	5	5	0	5	10	15	20
1.25	5	5	0	5	10	15	20
0.75	5	5	0	5	10	15	20
0.3	5	5	0	5	10	15	20
1	40	40	0	5	10	15	20
1.5	40	40	0	5	10	15	20

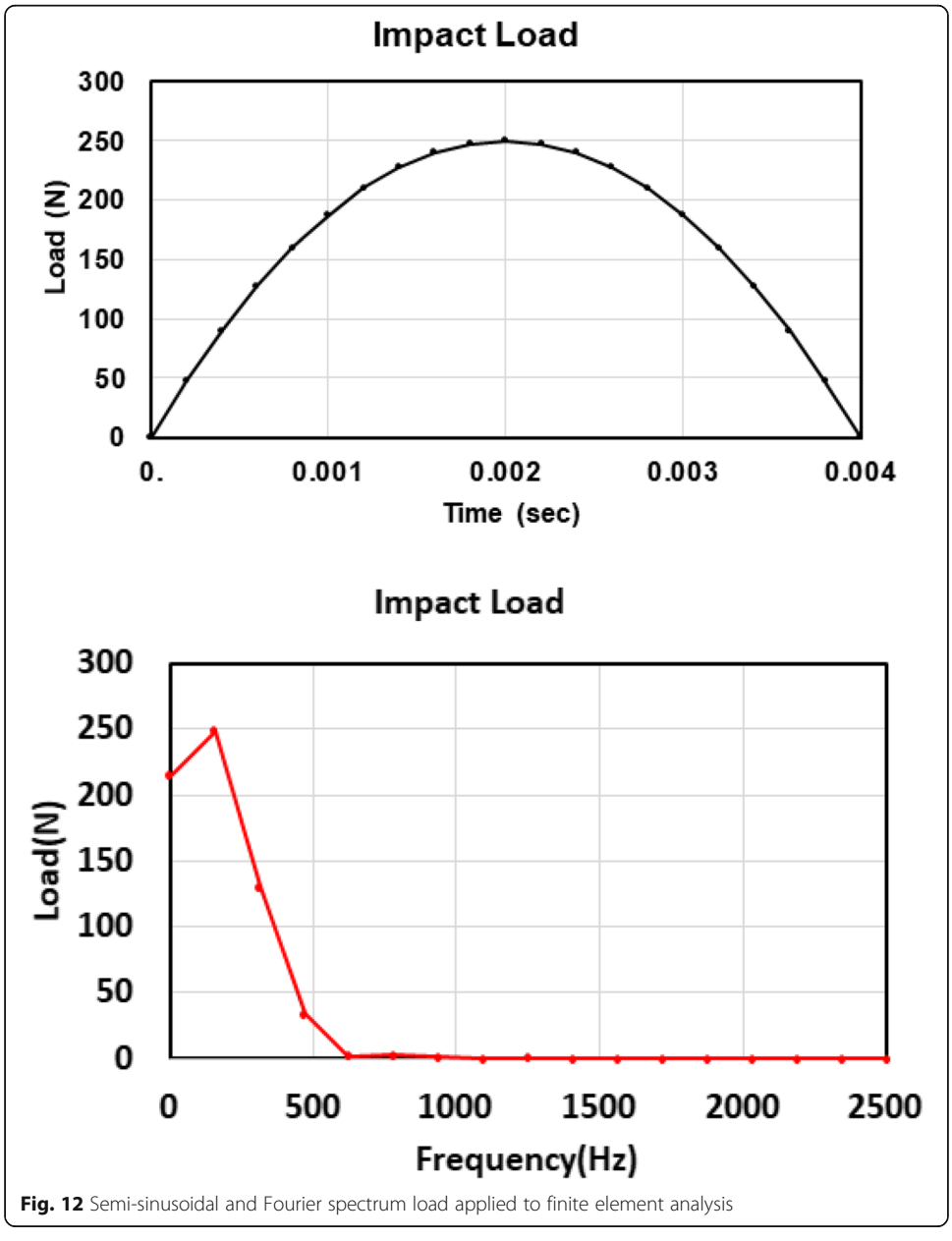

Fig. 12 Semi-sinusoidal and Fourier spectrum load applied to finite element analysis

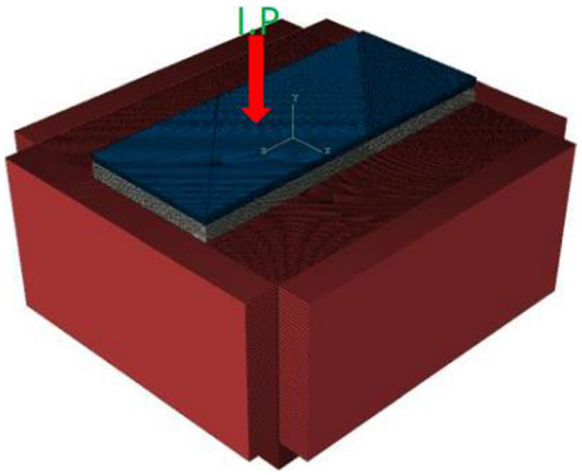

Fig. 13 Schematic for the impact load on a concrete slab track by 3D Abaqus

explained and confirmed that where there was no cavity the relative amplitude of the peak frequency fd was approximately equal to zero and the resonance frequency remained constant for all sensing points.

According to Fig. 15, for all cases, it is clear that the first mode resonance frequency (fr) or return frequency peaks were still the same (whether or not there was a cavity) after impact loading. In addition, the relative amplitude of peak frequency (fr and fd) depended on a number of factors, such as the extent, depth, continuity, and location of cavities as well as the content of the impact loading.

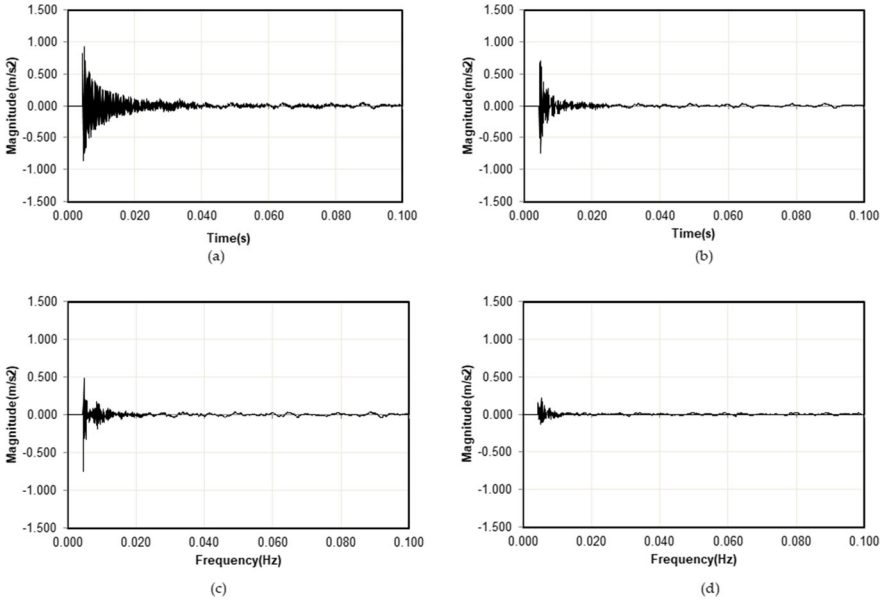

Fig. 14 Acceleration signals with time by cavity size. **a** 5 cm × 5 cm × 5 cm. **b** 5 cm × 5 cm × 1.25 cm. **c** 5 cm × 5 cm × 0.75 cm. **d** No cavity

Furthermore, when there was a shallow or less thick cavity as shown in Fig. 15d, the magnitude of the deck or peak frequency of fd above the cavity location was lower than fr. However, this time the result cannot be logically explained for this case, and it may be assumed that the shallow or less thick cavities under a concrete slab cannot cause a big effect on the concrete slab track depending on impact load applied on.

On the other hand, as it was expected and also revealed clearly in Fig. 15a, for a big, thick cavity, it can be easily seen that the magnitude of the deck or peak frequency of fd above the cavity location is much higher than the resonance frequency fr, we assumed to one of the reasons for a concrete slab track to fail.

FE results analysis by time frequency using the wavelet technique As we stated in the previous sections, the time-frequency analysis technique applied in this study was

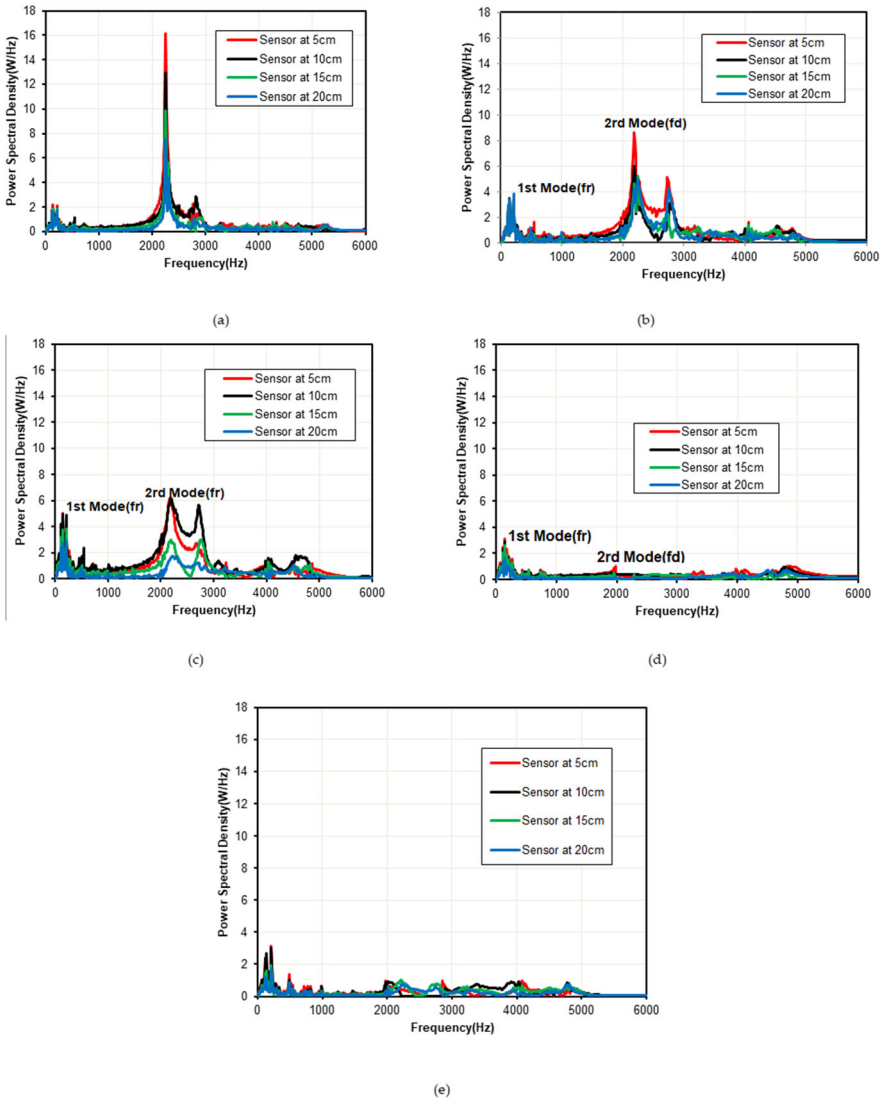

Fig. 15 Concrete slab track with cavity: **a** Cavity size 5 cm × 5 cm × 5 cm. **b** Cavity size 5 cm × 5 cm × 1.25 cm. **c** Cavity size 5 cm × 5 cm × 0.75 cm. **d** Cavity size 5 cm × 5 cm × 0.3 cm. **e** Non-cavity

Table 4 Summary of the FE results analytical analysis

Cavity size (cm)	TCL (cm)	HSB (cm)	T distance (cm)	d Distance (cm)	fr (Hz)	fd (Hz)
5 × 5 × 5	25	50	55.5	22.5	102	2342
5 × 5 × 1.25				24.375		2256
5 × 5 × 0.75				24.625		2144

the short-time Fourier transform (STFT) of the wavelet method. According to Ki-Il Song and Gye-Chun Cho [9, 17, 24], STFT is a technique for obtaining the segmented and filtered functions by applying the window function to each time band in order to show frequency characteristics over time and to perform the related Fourier transform.

The no cavity, small cavities, and big cavities cases were all simulated as it was stated in previous sections. The frequency response or the frequency reflection from cavity depth and the vibration resonance duration (TR) were obtained from short-time Fourier transform responses. These results are summarized in Tables 4 and 5.

As a typical result, the effects of the wavelet contours on the STFT responses are shown in Figs. 16, 17, 18, and 19. In the case of the no cavity condition (Fig. 16), the

Table 5 FEA results' summary for cavity and non-cavity conditions

Cavity size (cm)			Sensor location (cm)	Frequency response (Hz)	Resonance duration (S)	Volume (cm^3)	Ratio= ΔX/ΔY	I= ΔPSD/ (ΔY*ΔX) (W/HzS)	Observation
L	W	D							
5	5	5	5	2420	0.018133206	18567.52	3.14	1690326	Cavity condition
5	5	5	10	2420	0.016119153	14842.93	3.117	1520670	Cavity condition
5	5	5	15	2420	0.011572216	12494.80948	2.633	1291115	Cavity condition
5	5	5	20	2420	0.009080399	10347.7319	1.837	1054919	Cavity condition
5	5	5	25	2420	0.008152887	9648.570873	1.266	985304.5	Cavity condition
5	5	1.25	5	2250	0.013833206	11315.75118	2.361	1332777	Cavity condition
5	5	1.25	10	2250	0.012119153	9515.772963	2.786	1119797	Cavity condition
5	5	1.25	15	2250	0.009722158	7933.948132	2.167	1009318	Cavity condition
5	5	1.25	20	2250	0.009080399	6748.995931	1.837	903218.6	Cavity condition
5	5	1.25	25	2250	0.008152887	6211.697865	0.803	793179.3	Fair condition
5	5	0.75	5	2178	0.01161351	7878.323055	1.371	929964.7	Cavity condition
5	5	0.75	10	2178	0.008381138	7189.101855	1.05	791446.4	Fair condition
5	5	0.75	15	2178	0.006826848	6658.593746	0.856	649308.4	Fair condition
5	5	0.75	20	2178	0.006592786	6099.384799	0.796	648325.7	Fair condition
5	5	0.75	25	2178	0.006382283	5482.158766	0.629	590533.7	Good condition
5	5	0.3	5	2124	0.009028469	4112.444302	1.05	824824.7	Fair condition
5	5	0.3	10	2124	0.008932686	3989.324802	0.858	607984.9	Fair condition
5	5	0.3	15	2124	0.007591469	3589.617629	0.737	575679.6	Good condition
5	5	0.3	20	2124	0.005950318	3298.131422	0.645	559388.5	Good condition
5	5	0.3	25	2124	0.005942065	3294.030099	0.558	530918.6	Good condition
Non-cavity			5	2112	0.004680945	3683.685677	0.711	433452.2	Good condition
Non-cavity			10	2112	0.004532605	3253.757776	0.646	426242	Good condition
Non-cavity			15	2112	0.004271587	3013.219011	0.558	412116.1	Good condition
Non-cavity			20	2112	0.004214606	2808.013438	0.475	399226.9	Good condition
Non-cavity			25	2112	0.003906566	2773.609004	0.45	393622.1	Good condition

contour shape is non-symmetric and stretched parallel to the frequency axis. In the case of the small size of cavities condition (Fig. 19), the contour plot forms a circular (symmetrical) shape with small tails on both the time and frequency axes. The TR value is slightly longer than the case of no cavity condition; the frequency response value is 2124kHz. In the case of the big size of cavity condition (Fig. 17), the contour line is non-symmetric and stretches along the time axis within a dominant frequency range. The TR value is 0.018s longer than the duration shown in the case of no cavity and small size of cavities; the frequency response value is 2420Hz. The STFT response obtain here were also compared the Ki-Il Song and Gye-Chun Cho research [8] and also wavelet analysis result from field in the "Field test of an impact echo testing system" section (see Fig. 8).

For each case, the fd and TR value obtained from the short-time Fourier transform analyses are summarized in Table 5. As it is clearly seen in Table 5, the frequency response remains constant for each case (in here the sensors were only changed to different positions but impact load position was not changed), contrary the TR values decrease regarding the sensors' position.

Furthermore, the wavelet contours ratio (Δx/Δy) in this research have been also checked and calculated by matlab program as shown in Table 5 and Fig. 28; Δx has been considered as time axis and Δy as frequency axis. Therefore, the calculated ratios have been divided into three conditions, such as Cavity condition, Fair condition (where there is small cavity), and also non-cavity condition. All obtained results are summarized in Table 5.

In summary, as the cavity condition worsens (from Figs. 16, 17, 18, and 19), the fd and TR values increase and the shape of the contour plot changes. Thus, the presence of cavity under concrete slab track can be clearly identified with STFT responses, which

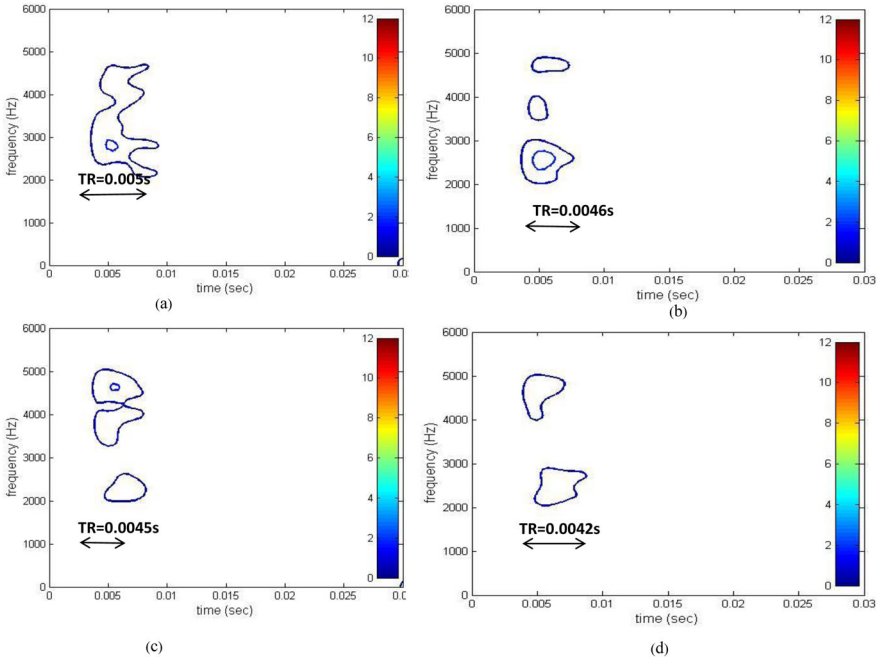

Fig. 16 Case 1: no cavity. **a** Sensor at 5 cm. **b** Sensor at 10 cm. **c** Sensor at 15 cm. **d** Sensor at 20 cm

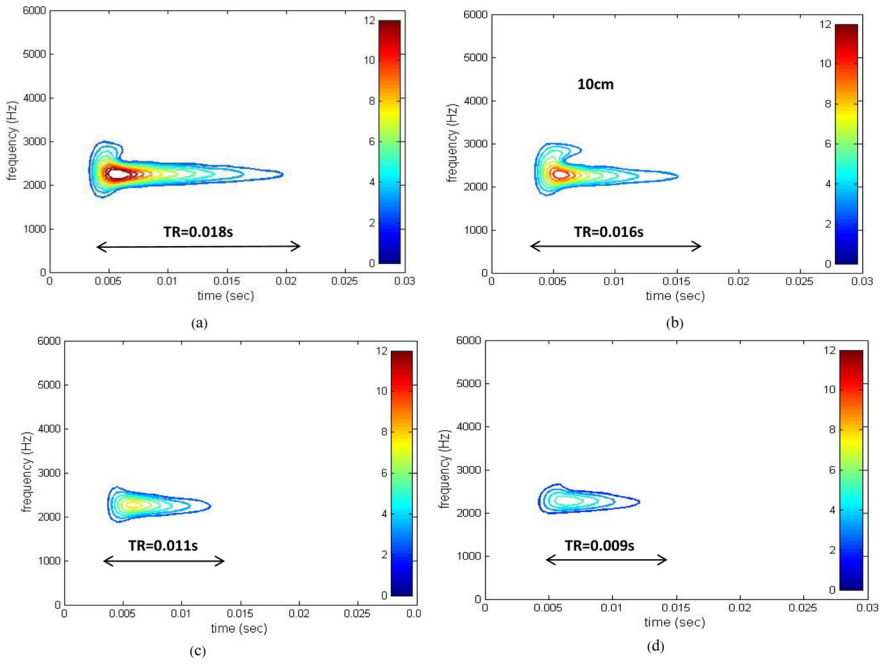

Fig. 17 Case 2: cavity size 5 × 5 × 5cm. **a** Sensor at 5 cm. **b** Sensor at 10 cm. **c** Sensor at 15 cm. **d** Sensor at 20 cm

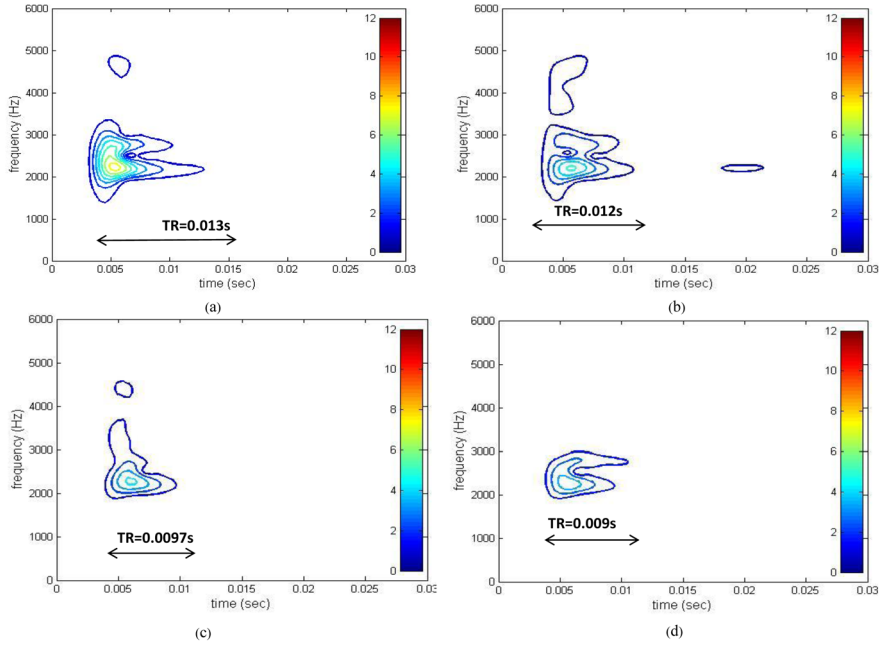

Fig. 18 Case 3: cavity size 5 × 5 × 1.25 cm. **a** Sensor at 5 cm. **b** Sensor at 10 cm. **c** Sensor at 15 cm. **d** Sensor at 20 cm

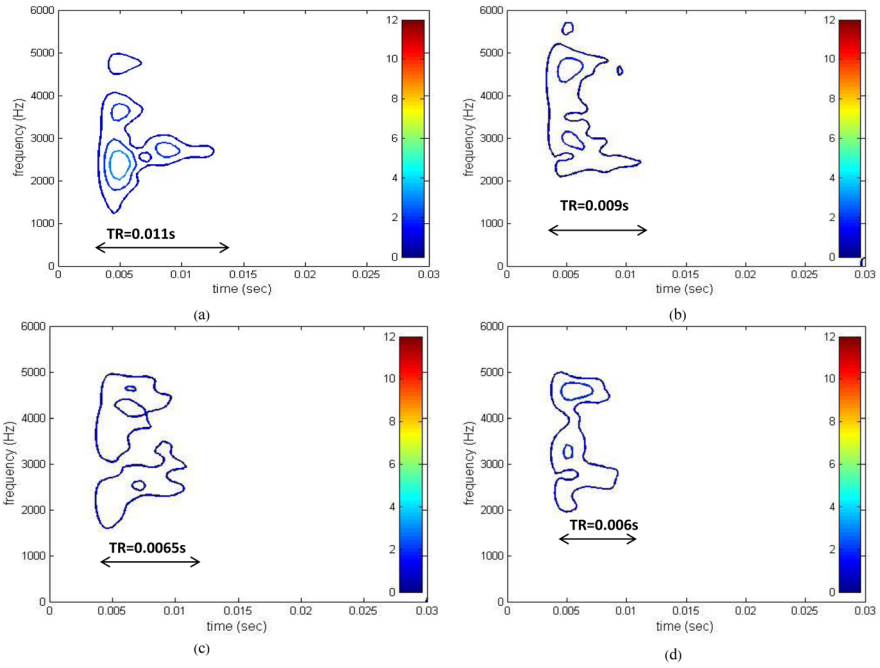

Fig. 19 Case 4: cavity size 5 × 5 × 0.75 cm. **a** Sensor at 5 cm. **b** Sensor at 10 cm. **c** Sensor at 15 cm. **d** Sensor at 20 cm

show a relatively long tail parallel to the time axis regardless of the cavity cases. This response can also be observed in the case of a no cavity or small cavities condition.

Verification of cavities by analytical analysis This section reports the analytical results from different sizes of cavity (see Fig. 15a, b, e) that were obtained by following the method as used by Gucunski et al. [11] to determine fd and fr for three types of

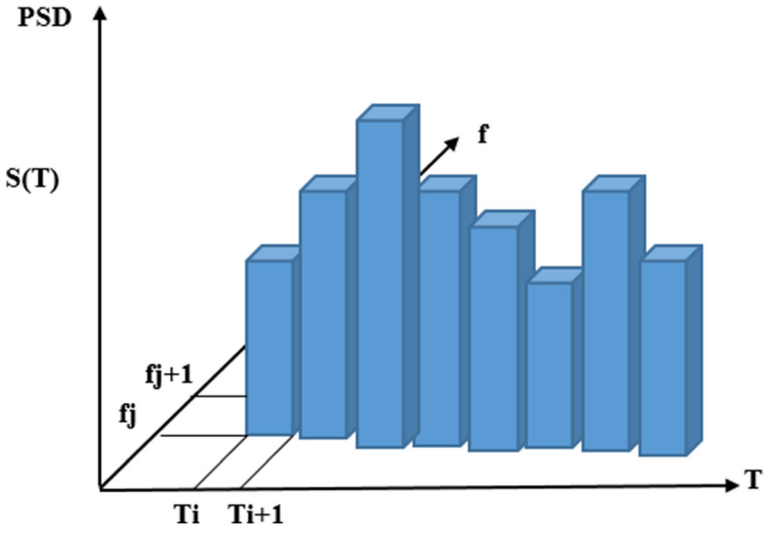

Fig. 20 Schematic for spectrum height with frequency and period intervals

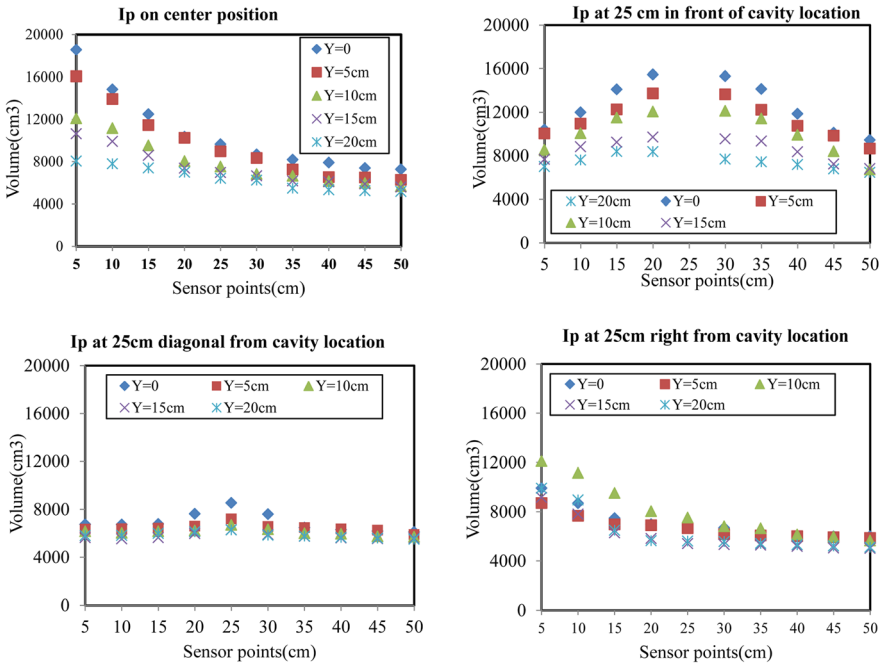

Fig. 21 Volume analysis for cavity size 5 × 5 × 5

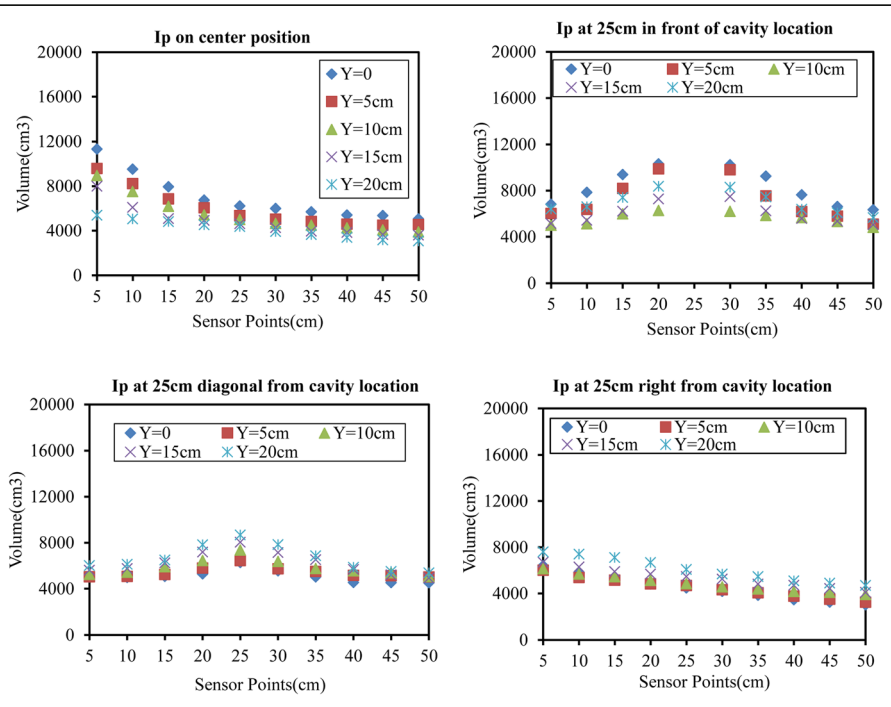

Fig. 22 Volume analysis for cavity size 5 × 5 × 1.25

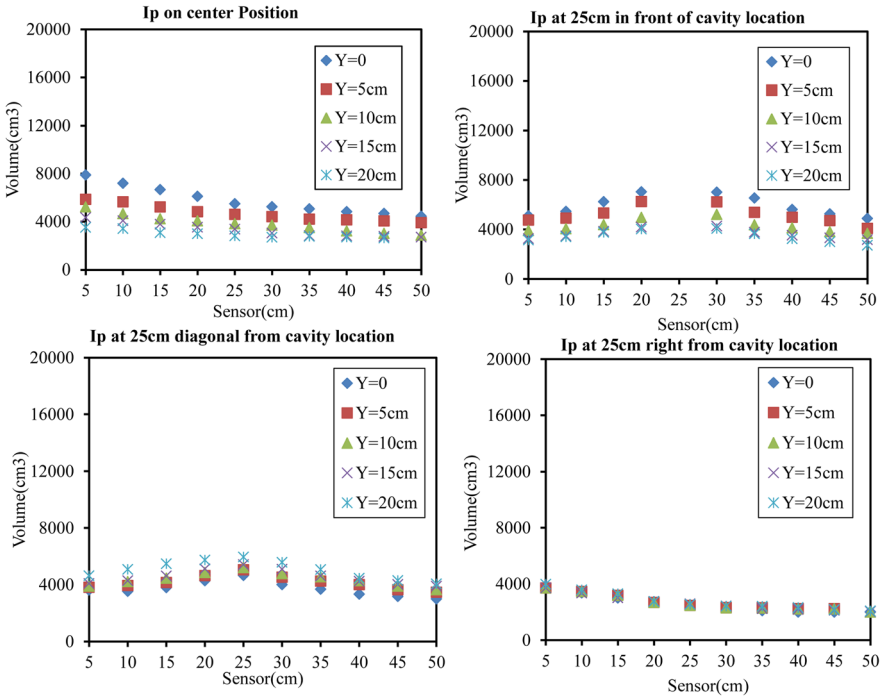

Fig. 23 Volume analysis for cavity size 5 × 5 × 0.75

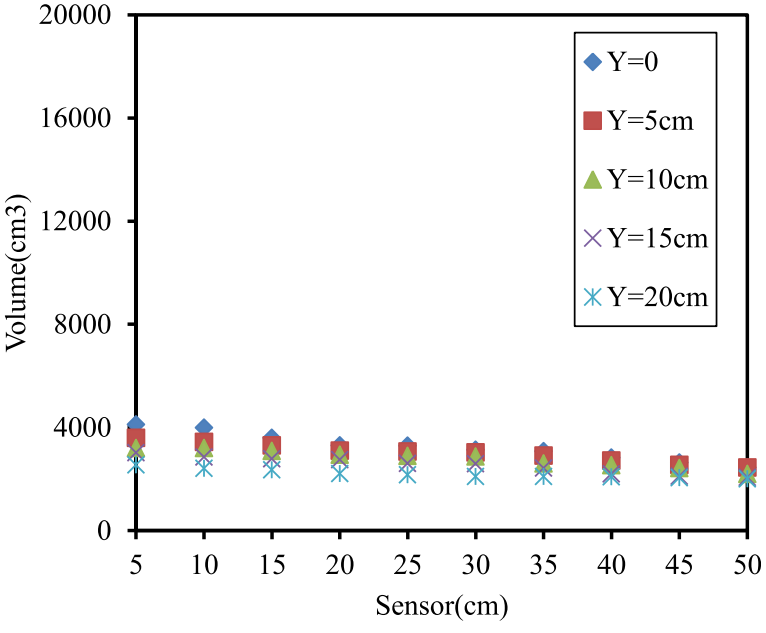

Fig. 24 Volume analysis for non-cavity condition

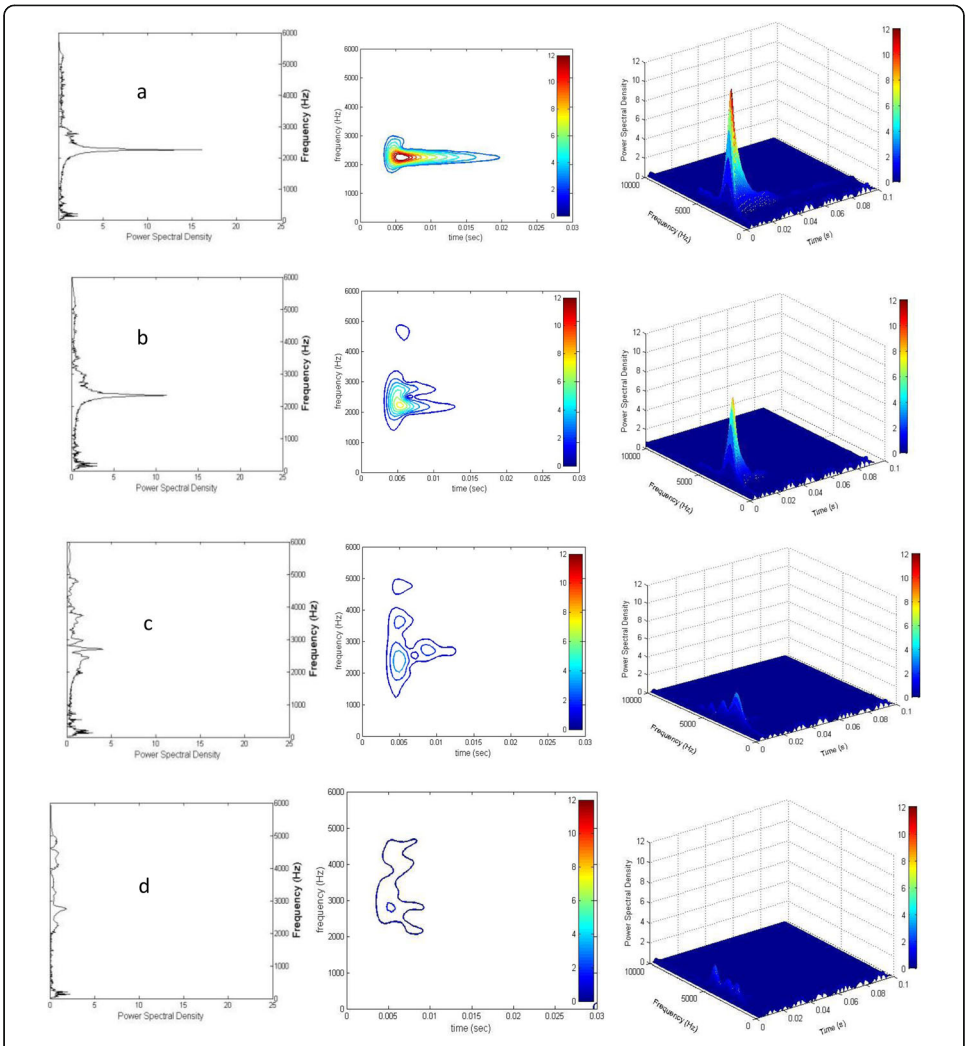

Fig. 25 Comparison of different cases of cavities by mountain shape: **a** 5 × 5 × 5cm. **b** 5 × 5 × 1.25cm. **c** 5 × 5 × 0.75cm. **d** No cavity

cavity condition; the results were then compared to the results obtained from the FE results (Fig. 20).

Equations 5 and 6 were used to calculate the fd and fr peak values. The obtained values are summarized in Table 4.

$$f_r = \frac{V_P}{2T} \tag{5}$$

$$f_d = \frac{V_P}{2d} \tag{6}$$

Wave speed Vp: 1100m/s T is the distance between the impact surface and the lower surface where there is no cavity (see Fig. 12), and d is the distance from the impact surface to the top of the cavity. (This wave speed was also used in the impact echo system mentioned in previous sections.)

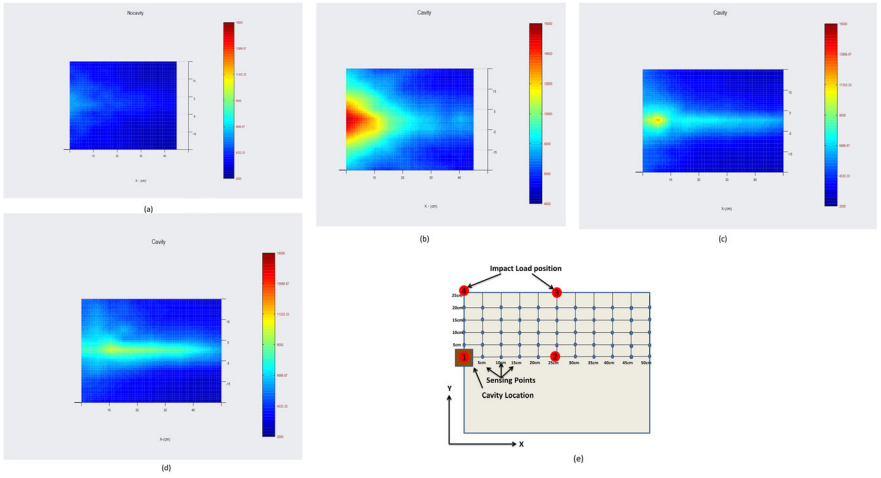

Fig. 26 Verification of the cavity using PSD values: **a** Ip on center where there is no cavity. **b** Ip on center where there is a cavity. **c** Impact load at 5cm from the cavity location. **d** Impact load at 10cm from the cavity location. **e** Concrete slab track sensing points

Verification of cavity by volume Using Mat lab software, we calculated the volume of peak frequency values for sensing points and by Eq. 7, and Figs. 21, 22, 23, and 24 give the obtained results. Logically, we can confirm that the bigger the size of the cavity, the bigger the volume of the peak sensing point (see Table 5).

On the other hand, the volume results of the cavity cases which were calculated for the different position of impact load (see Fig. 26e) show clearly very important explanation that the big size of cavity and its impact under concrete slab track can be observed in different position (see Fig. 21).

Furthermore, it is clear that the farther the distance from the location of the cavity beneath the concrete slab, the more the volume values for the sensing points decrease.

$$V = \sum_{i=0}^{n} \int_{T_i}^{T_{i+1}} \sum_{i=0}^{n} \int_{f_j}^{f+1} S(T) dT df \tag{7}$$

where
f = frequency
T = time
S(T) = power spectrum density
n = number of period intervals
m = number of frequency intervals

Verification of mountain shapes for different cases of cavity Considering Fig. 25, we used the cavity mountain shape as a complementary tool for studying the effect of cavities. Using this technique, we can illustrate changes in volume and mountain shape in a three-dimensional time, frequency, and auto spectrum density. The results make it clear that the bigger the size of the cavity the bigger the shape of the mountain. On the other hand, where there is no cavity, it is very difficult to identify whether there is a mountain shape or not because the PSD values are very small.

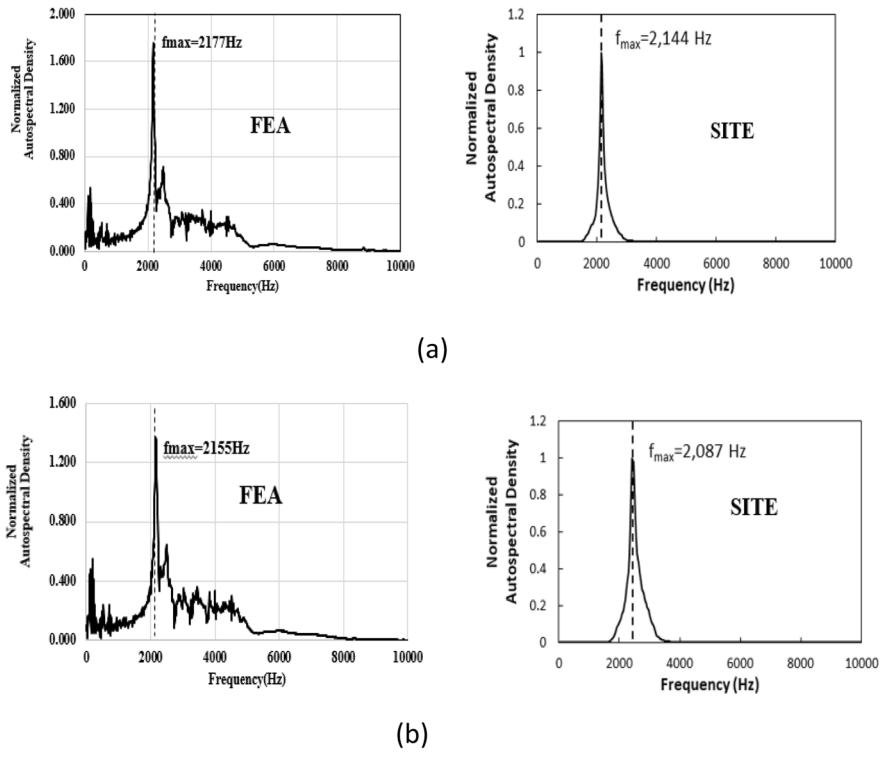

Fig. 27 Comparison of results from the FEA and site testing: **a** Cavity size (40 cm × 40 cm × 1.5 cm). **b** Cavity size (40 cm × 40 cm × 1 cm)

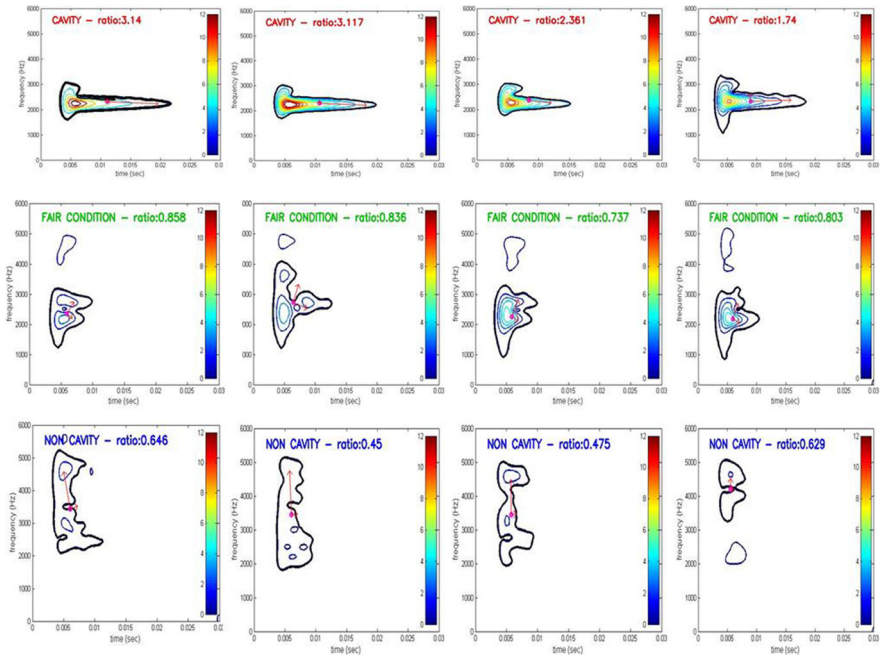

Fig. 28 Verification of cavity by using wavelet contours ratio (Δx/Δy)

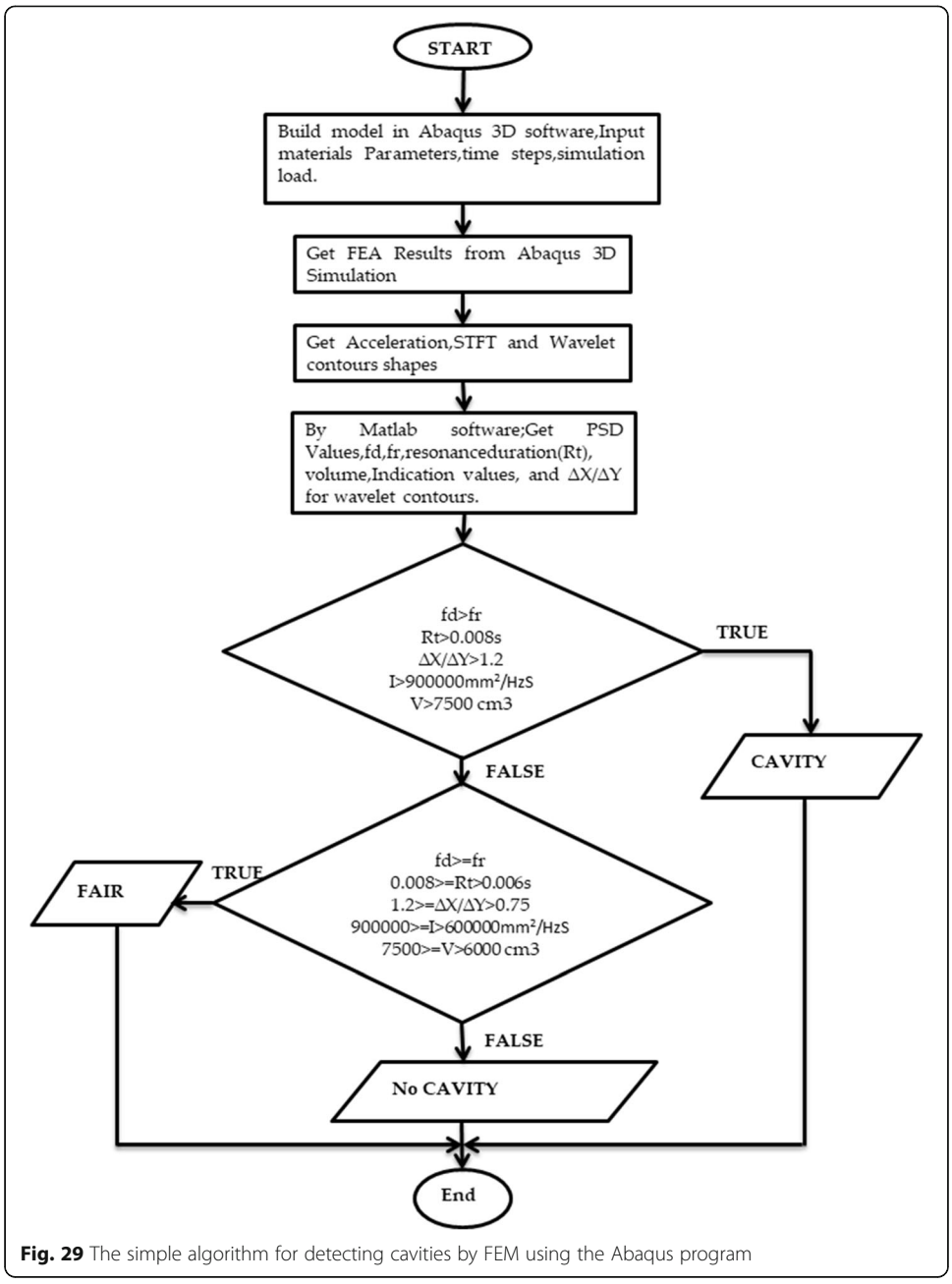

Fig. 29 The simple algorithm for detecting cavities by FEM using the Abaqus program

Therefore, a 3D time-frequency-PSD representation of the cavity mountain shape provides an opportunity to distinguish the presence of cavities under concrete slabs, which may go undetected in the STFT-based averaged spectrum.

Verification of a cavity using PSD values Another point was verification of cavities by checking the PSD values for all sensing points located on the given concrete slab tracks. All sensing points are presented in Fig. 26e. Matlab program and MS Excel were used to calculate the PSD values for each sensing point and these PSD values have been used for calculating indication values (see Table 5). In Fig. 26a, there is no red color,

which means that the there is no cavity. Figure 26b demonstrates the effect of the impact load on top of a cavity. The comparison of Fig. 26c and d with Fig. 26a clearly demonstrates and distinguishes the influence of the presence of a cavity under the concrete slab track.

Site and FEA results comparison

As shown in Fig. 27, the cavity size of 40cm × 40cm × 1.5cm and 40cm × 40cm × 1cm were modeled and simulated in 3D Abaqus software.

On the site located at Dong Yang University, a railway concrete slab track was constructed and then the same size cavities used in the Abaqus models were also excavated between the TCL and the HSB. The impact echo system device developed in this study was used to detect cavities under the concrete slab track on the site and its results were compared to the results obtained by the finite element method.

In general, the maximum peak frequency of FEM results has a little difference of about 1.5% compared to the results from the site. That difference was likely caused by the filtering techniques used to analyze the site results and also the timing of the impact echo system device users. Another cause would likely be the material used to represent the cavity underneath the concrete slab track on the site because for the FEM we only made a hole between the TCL and the HSB to consider as cavities in the Abaqus simulation.

It is also clearly seen in Fig. 27 that the figures of the site results are very clearer and smoother than FEM results; this occurred because in analyzing the site results, we focused only on the maximum frequency, which had peak values, and therefore the considered acceleration time was in intervals of −0.01 to 0.02 s. Contrary to the FEM results where were not filtered because in the FEA results we wanted to determine both the resonance frequency and the maximum peak value of the frequency from the cavity depth (Fig. 28).

Simple algorithm for detecting cavities by FEM

Figure 29 illustrates the simple algorithm for detecting cavities by FEM using the Abaqus program. The input parameters are physical and structure parameters that must be considered to simulate the TCL, HSB, soil, and impact load. The STFT and wavelet equation is simply represented by Eq. 4. The algorithm can also consider the PSD, resonance duration, volume and indication values, and the wavelet shape size (ratio) as well as magnitude of fd and fr.

Conclusion

This study developed a nondestructive testing method to predict cavities under concrete slabs using a concrete track defect measurement system and the finite element method. Some important results from this study are summarized as follows:

◦ The concrete track defect measurement system consists of two models: a handy type solenoid and a main body. The handy type solenoid is composed of an impact source (solenoid) and an impact source control switch. The vibration sensing device (acceleration sensor) consists of a data measurement system (NI chassis, NI DAQ, small

PC, 7-inch capacitive touch screen) and a power supply (built-in battery, step-up module, step down module, power switch and battery residual indicator).
◦ Data acquisition and the analysis program for the impact echo test was developed using a Matlab program.
◦ For the field test of the concrete track defect measurement system, wood block panels 400 mm in width and 5, 10, and 15 mm in thickness were placed between the TCL and the HSB layer of the concrete slab track. If there was an abnormality between the TCL and HSB layers at the site, the impact echo technique developed in this study could measure and confirm the abnormality, and the depth of cavity could be calculated and determined.
◦ The FEA program ABAQUS successfully performed a numerical analysis of the impact echo test in 3D for the concrete slab track to determine whether or not there were cavities under the concrete slab track.
◦ Multiple verifications were performed to determine whether there were cavities by STFT, volume, PSD values, and site testing results. All those verifications confirmed the expected results from the cavity locations.
◦ The FEA results confirmed that with an increase in the cavity height, the frequency of reflections from the cavity depth (fd) also increases. In the 3D modeling, the frequency of the reflections from the cavity depth of the concrete slab track with a cavity size of 5cm × 5cm × 5cm was 2342Hz; for a cavity size of 5cm × 5cm × 1.25cm, it was fd= 2256Hz; and for a cavity size of 5cm × 5cm × 0.75cm, it was fd =2145Hz. In addition to the FEA results, the resonant frequency for all the cases, whether there were cavities or no cavities, was constant and equal to 102Hz.

We concluded that the impact echo technique developed in this study with FEA can measure and confirm the location of cavities in concrete slabs, and also the depth of cavities can be calculated and determined. In addition, the method can also be used to check and compare the results from sites.

Abbreviations

NDT: Nondestructive testing; 3D: Three dimension; FEA: Finite element analysis; TCL: Track concrete layer; HSB: Hydraulically stabilized base; FFT: Fast Fourier transform; STFT: Short-time Fourier transform; FDTD: Finite difference time domain; FEM: Finite element method; *P*: Compressive wave; *S*: Shear wave; *V*: Velocity; *G*: Stiffness; *ρ*: Mass density; Vp: The propagation velocity; *f*: Frequency; fr: Resonance frequency; fd: Peak frequency; λ: Wavelength; *d*: Depth or thickness of concrete slab; *β*: Shape coefficient; *S* (f): Auto spectrum density; *E*: Expected energy; XT (f): Fourier transform value; *T*: Time; TR: Vibration resonance duration; S(T) or PSD: Power spectrum density; *n*: Number of period intervals; *m*: Number of frequency intervals

Acknowledgements

Not applicable.

Authors' contributions

PAB: correcting data, testing, analyzing data, writing manuscript. LDV: correcting data, performed data from software. YL: overall supervisor of this paper research and was a major contributor in writing the manuscript. All authors read and approved the final manuscript.

Funding

All funding for this research has been paid by the authors.

Availability of data and materials

All materials and data used should be available at PaiChai University/South Korea.
The datasets used and/or analyzed during the current study are available from the corresponding author on reasonable request.

Declarations

Competing interests

The authors have declared no conflict of interests for this research.

Received: 1 April 2021 Accepted: 21 June 2021
Published online: 01 September 2021

References

1. Pierre AB (2019) Performance evaluation of impact echo method for detection of cavity underneath a concrete slab track using finite element method. Master's Thesis, Pai Chai University, Daejeon
2. Michas G (2012) Slab track systems for high-speed railways. Master Thesis, School of Architecture and the Built Environment, Royal Institute of Technology, Stockholm
3. Esveld C (2001) Modern railway track, 2nd edn. Delft University of Technology, Delft
4. Lim Y, Park S, Cho H, Park J (2019) Comparison of conventional and acoustic impact echo tests for detecting a cavity underneath a concrete slab track. WIT Trans Built Environ 181:499–506
5. Sansalone M (1997) Impact-echo: the complete story. ACI Struct J 94:777–786
6. Ohtsu M, Watanabe T (2002) Stack imaging of spectral amplitudes based on impact-echo for flaw detection. NDT E Int 35:189–196
7. Oh T, Popovics JS, Ham S, Shin SW (2013) Improved interpretation of vibration responses from concrete delamination defects using air-coupled impact resonance tests. J Eng Mech 139:315–324
8. Melhem H, Kim H (2003) Damage detection in concrete by Fourier and wavelet analyses. J Eng Mech 129:571–577
9. Song K, Cho G (2010) Numerical study on the evaluation of tunnel shotcrete using the impact-echo method coupled with Fourier transform and short-time Fourier transform. Intl J Rock Mech Min Sci 47(8):1274–1288. https://doi.org/10.1016/j.ijrmms.2010.09.005
10. Gabor D (1946) Theory of communication. J EEE 93:429–457
11. Shokouhi P, Gucunski N, Maher A (2006) Time-frequency techniques for impact echo data analysis and interpretations. 9th European Conference on NDT, Berlin
12. Sansalone M, Carino NJ (1986) Impact-echo: a method for flaw detection in concrete using transient stress waves. National Bureau of Standards, Springfield
13. Carino N, Sansalone M (1992) Detection of voids in grouted ducts using the impact-echo method. ACI Mater J 89:296–303
14. Cheng C, Sansalone M (1993) Effects on impact-echo signals caused by steel reinforcing bars and voids around bars. ACI Mater J 90:421–434
15. Santamarina J, Fratta D (1998) Introduction to discrete signals and inverse problems in civil engineering. ASCE Press, Reston, p 327
16. Carino N (2013) Training: often the missing link in using NDT methods. Construct Build Mater 38:1316–1329. https://doi.org/10.1016/j.conbuildmat.2011.03.060
17. Newland D (1999) Ridge and phase identification in the frequency analysis of transient signals by harmonic wavelets. J Vib Acoust 121(2):149–155. https://doi.org/10.1115/1.2893957
18. Rail One. Rheda ballastless track system. Available online: http://www.railone.com. Accessed 21 Dec 2019.
19. Tayabji S, Bilow D (2000) Concrete slab track state of the practice. TRR 1742:87–96
20. Darr E, Fiebig W (2006) Feste Fahrbahn: Konstruktion und Bauarten für Eisenbahn und Strassenbahn (Deutsch), 2nd edn. Eurailpress, Germany
21. Profillidis V (2006) Railway management and engineering, 3rd edn. Ashgate Publishing Limited, New York
22. Franz Q (2001) Innovative track systems technical construction. Project funded by the European Community, Directorate General Energy and Transport Under the Competitive and Sustainable Growth Program, ProMain, TÜV Intertraffic, Cologne
23. Kwon S, Park M, Kim D, Sho B, Park J (2014) Correlation analysis between crack and TQI in RC slab track. IJR 7(1):8–15. https://doi.org/10.7782/IJR.2014.7.1.008
24. Torrence C, Compo G (1998) A practical guide to wavelet analysis. Bull Am Meteorol Soc 79(1):61–78. https://doi.org/10.1175/1520-0477(1998)0790061:APGTWA2.0.CO;2

Publisher's Note